High-temperature stable π-phase-shifted fiber Bragg gratings inscribed using infrared femtosecond pulses and a phase mask

Hnatovsky, Cyril; Grobnic, Dan; Mihailov, Stephen J.

Publisher's version / Version de l'éditeur:
https://doi.org/10.1364/OE.26.023550
Optics Express, 26, 18, pp. 23550-23564, 2018

Research Article | Vol. 26, No. 18 | 3 Sep 2018 | OPTICS EXPRESS 23550
Optics EXPRESS

High-temperature stable π-phase-shifted fiber Bragg gratings inscribed using infrared femtosecond pulses and a phase mask

CYRIL HNATOVSKY,* DAN GROBNIC, AND STEPHEN J. MIHAILOV

National Research Council of Canada, Security and Disruptive Technologies, 100 Sussex Dr., Ottawa, ON, K1A 0R6, Canada
Cyril.Hnatovsky@nrc-cnrc.gc.ca

Abstract: Type II π-phase-shifted Bragg gratings stable up to ~1000°C are written inside a standard single mode silica optical fiber (SMF-28) with infrared femtosecond pulses and a special phase mask. Inscription through the protective polyimide fiber coating is also demonstrated. The birefringence of the Bragg gratings and, as a result, the polarization dependence of their spectra are strongly affected by the femtosecond laser polarization. Using optimized writing conditions, the full width at half maximum of the π-phase-shifted passband feature can be ~30 pm in transmission, while the polarization-dependent shift of its central wavelength can be less than 8 pm, for a 7 mm long grating structure. This makes such gratings a unique tool for high-resolution measurements of temperature, load and vibration in extreme temperature environments.

OCIS codes: (060.3738) Fiber Bragg gratings, photosensitivity; (060.7140) Ultrafast processes in fibers; (140.3390) Laser materials processing.

References and links

1. X. Chen, J. Yao, F. Zeng, and Z. Deng, "Single-longitudinal-mode fiber ring laser employing an equivalent phase-shifted fiber Bragg grating," IEEE Photonics Technol. Lett. **17**(7), 1390–1392 (2005).
2. S. A. Babin, D. V. Churkin, A. E. Ismagulov, S. I. Kablukov, and M. A. Nikulin, "Single frequency single polarization DFB fiber laser," Laser Phys. Lett. **4**(6), 428–432 (2007).
3. M. LeBlanc, S. T. Vohra, T. E. Tsai, and E. J. Friebele, "Transverse load sensing by use of pi-phase-shifted fiber Bragg gratings," Opt. Lett. **24**(16), 1091–1093 (1999).
4. D. Gatti, G. Galzerano, D. Janner, S. Longhi, and P. Laporta, "Fiber strain sensor based on a π-phase-shifted Bragg grating and the Pound-Drever-Hall technique," Opt. Express **16**(3), 1945–1950 (2008).
5. Q. Zhang, N. Liu, T. Fink, H. Li, W. Peng, and M. Han, "Fiber-optic pressure sensor based on π-phase-shifted fiber Bragg grating on side-hole fiber," IEEE Photonics Technol. Lett. **24**(17), 1519–1522 (2012).
6. B. Huang and X. Shu, "Ultra-compact strain- and temperature-insensitive torsion sensor based on a line-by-line inscribed phase-shifted FBG," Opt. Express **24**(16), 17670–17679 (2016).
7. A. Rosenthal, D. Razansky, and V. Ntziachristos, "High-sensitivity compact ultrasonic detector based on a pi-phase-shifted fiber Bragg grating," Opt. Lett. **36**(10), 1833–1835 (2011).
8. G. P. Agrawal and S. Radic, "Phase-shifted fiber Bragg gratings and their application for wavelength demultiplexing," IEEE Photonics Technol. Lett. **6**(8), 995–997 (1994).
9. A. Melloni, M. Chinello, and M. Martinelli, "All-optical switching in phase-shifted fiber Bragg grating," IEEE Photonics Technol. Lett. **12**(1), 42–44 (2000).
10. N. K. Berger, B. Levit, B. Fischer, M. Kulishov, D. V. Plant, and J. Azaña, "Temporal differentiation of optical signals using a phase-shifted fiber Bragg grating," Opt. Express **15**(2), 371–381 (2007).
11. J. Canning and M. G. Sceats, "π-phase-shifted periodic distributed structures in optical fibres by UV post-processing," Electron. Lett. **30**(16), 1344–1345 (1994).
12. P. F. Mckee, R. Kashyap, and D. Armes, "UV written reflection grating structures in photosensitive optical fibres using phase-shifted phase masks," Electron. Lett. **30**(23), 1977–1978 (1994).
13. W. H. Loh, M. J. Cole, M. N. Zervas, S. Barcelos, and R. I. Laming, "Complex grating structures with uniform phase masks based on the moving fiber-scanning beam technique," Opt. Lett. **20**(20), 2051–2053 (1995).
14. G. D. Marshall, R. J. Williams, N. Jovanovic, M. J. Steel, and M. J. Withford, "Point-by-point written fiber-Bragg gratings and their application in complex grating designs," Opt. Express **18**(19), 19844–19859 (2010).
15. J. Burgmeier, C. Waltermann, G. Flachenecker, and W. Schade, "Point-by-point inscription of phase-shifted fiber Bragg gratings with electro-optic amplitude modulated femtosecond laser pulses," Opt. Lett. **39**(3), 540–543 (2014).

#336581 https://doi.org/10.1364/OE.26.023550
Journal © 2018 Received 2 Jul 2018; revised 13 Aug 2018; accepted 20 Aug 2018; published 28 Aug 2018

Optics EXPRESS

16. M. Bernier, V. Michaud-Belleau, S. Levasseur, V. Fortin, J. Genest, and R. Vallée, "All-fiber DFB laser operating at 2.8 μm," Opt. Lett. **40**(1), 81–84 (2015).
17. A. Shamir and A. A. Ishaaya, "Femtosecond inscription of phase-shifted gratings by overlaid fiber Bragg gratings," Opt. Lett. **41**(9), 2017–2020 (2016).
18. J. He, Y. Wang, C. Liao, Q. Wang, K. Yang, B. Sun, G. Yin, S. Liu, J. Zhou, and J. Zhao, "Highly birefringent phase-shifted fiber Bragg gratings inscribed with femtosecond laser," Opt. Lett. **40**(9), 2008–2011 (2015).
19. Y. Du, T. Chen, Y. Zhang, R. Wang, H. Cao, and K. Li, "Fabrication of phase-shifted fiber Bragg grating by femtosecond laser shield method," IEEE Photonics Technol. Lett. **29**(24), 2143–2146 (2017).
20. Y. Jiang, C. Liu, D. Li, D. Yang, and J. Zhao, "Simultaneous measurement of temperature and strain using a phase-shifted fiber Bragg grating inscribed by femtosecond laser," Meas. Sci. Technol. **29**(4), 045101 (2018).
21. S. J. Mihailov, D. Grobnic, C. W. Smelser, P. Lu, R. B. Walker, and H. Ding, "Bragg grating inscription in various optical fibers with femtosecond infrared lasers and a phase mask," Opt. Mater. Express **1**(4), 754–765 (2011).
22. A. Martinez, I. Y. Khrushchev, and I. Bennion, "Direct inscription of Bragg gratings in coated fibers by an infrared femtosecond laser," Opt. Lett. **31**(11), 1603–1605 (2006).
23. S. J. Mihailov, D. Grobnic, and C. W. Smelser, "Efficient grating writing through fibre coating with femtosecond IR radiation and phase mask," Electron. Lett. **43**(8), 442–443 (2007).
24. D. Grobnic, S. J. Mihailov, C. W. Smelser, and R. T. Ramos, "Ultrafast IR laser writing of strong Bragg gratings through the coating of high Ge-doped optical fibers," IEEE Photonics Technol. Lett. **20**(12), 973–975 (2008).
25. S. J. Mihailov, D. Grobnic, R. B. Walker, C. W. Smelser, G. Cuglietta, T. Graver, and A. Mendez, "Bragg grating writing through the polyimide coating of high NA optical fibres with femtosecond IR radiation," Opt. Commun. **281**(21), 5344–5348 (2008).
26. M. Bernier, F. Trépanier, J. Carrier, and R. Vallée, "High mechanical strength fiber Bragg gratings made with infrared femtosecond pulses and a phase mask," Opt. Lett. **39**(12), 3646–3649 (2014).
27. D. Grobnic, C. Hnatovsky, and S. J. Mihailov, "Thermally stable type II FBGs written through polyimide coatings of silica-based optical fiber," IEEE Photonics Technol. Lett. **29**(21), 1780–1783 (2017).
28. C. Hnatovsky, D. Grobnic, and S. J. Mihailov, "Through-the-coating femtosecond laser inscription of very short fiber Bragg gratings for acoustic and high temperature sensing applications," Opt. Express **25**(21), 25435–25446 (2017).
29. J. Habel, T. Boilard, J.-S. Frenière, F. Trépanier, and M. Bernier, "Femtosecond FBG Written through the Coating for Sensing Applications," Sensors (Basel) **17**(11), 2519 (2017).
30. V. V. Rondinella and M. J. Matthewson, "Effect of chemical stripping on the strength and surface morphology of fused silica optical fiber," Proc. SPIE **2074**, 52–58 (1994).
31. R. S. Robinson and H. H. Yuce, "Scanning tunneling microscopy of optical fiber corrosion: surface roughness contribution to zero-stress aging," J. Am. Ceram. Soc. **74**(4), 814–818 (1991).
32. P. Lu, D. Grobnic, and S. J. Mihailov, "Characterization of the birefringence in fiber Bragg gratings fabricated with an ultrafast-infrared laser," J. Lightwave Technol. **25**(3), 779–786 (2007).
33. L. A. Fernandes, J. R. Grenier, P. V. S. Marques, J. S. Aitchison, and P. R. Herman, "Strong birefringence tuning of optical waveguides with femtosecond laser irradiation of bulk fused silica and single mode fibers," J. Lightwave Technol. **31**(22), 3563–3569 (2013).
34. Y. Sheng, J. E. Rothenberg, H. Li, Y. Wang, and J. Zweiback, "Split of phase shifts in a phase mask for fiber Bragg gratings," IEEE Photonics Technol. Lett. **16**(5), 1316–1318 (2004).
35. Y. Sheng and L. Sun, "Near-field diffraction of irregular phase gratings with multiple phase-shifts," Opt. Express **13**(16), 6111–6116 (2005).
36. G. Tremblay and Y. Sheng, "Effects of the phase shift split on phase-shifted fiber Bragg gratings," J. Opt. Soc. Am. B **23**(8), 1511–1516 (2006).
37. C. Hnatovsky, D. Grobnic, D. Coulas, M. Barnes, and S. J. Mihailov, "Self-organized nanostructure formation during femtosecond-laser inscription of fiber Bragg gratings," Opt. Lett. **42**(3), 399–402 (2017).
38. C. W. Smelser, S. J. Mihailov, D. Grobnic, P. Lu, R. B. Walker, H. Ding, and X. Dai, "Multiple-beam interference patterns in optical fiber generated with ultrafast pulses and a phase mask," Opt. Lett. **29**(13), 1458–1460 (2004).
39. C. W. Smelser, D. Grobnic, and S. J. Mihailov, "Generation of pure two-beam interference grating structures in an optical fiber with a femtosecond infrared source and a phase mask," Opt. Lett. **29**(15), 1730–1732 (2004).
40. C. Smelser, S. Mihailov, and D. Grobnic, "Formation of Type I-IR and Type II-IR gratings with an ultrafast IR laser and a phase mask," Opt. Express **13**(14), 5377–5386 (2005).
41. R. J. Williams, R. G. Krämer, S. Nolte, M. J. Withford, and M. J. Steel, "Detuning in apodized point-by-point fiber Bragg gratings: insights into the grating morphology," Opt. Express **21**(22), 26854–26867 (2013).
42. S. J. Mihailov, "Fiber Bragg grating sensors for harsh environments," Sensors (Basel) **12**(2), 1898–1918 (2012).
43. J. Thomas, C. Voigtländer, R. G. Becker, D. Richter, A. Tünnermann, and S. Nolte, "Femtosecond pulse written fiber gratings: a new avenue to integrated fiber technology," Laser Photonics Rev. **6**(6), 709–723 (2012).
44. Y. Shimotsuma, P. G. Kazansky, J. Qiu, and K. Hirao, "Self-organized nanogratings in glass irradiated by ultrashort light pulses," Phys. Rev. Lett. **91**(24), 247405 (2003).
45. V. R. Bhardwaj, E. Simova, P. P. Rajeev, C. Hnatovsky, R. S. Taylor, D. M. Rayner, and P. B. Corkum, "Optically produced arrays of planar nanostructures inside fused silica," Phys. Rev. Lett. **96**(5), 057404 (2006).

Optics EXPRESS

46. Y. Shimotsuma, K. Hirao, J. Qiu, and P. G. Kazansky, "Nano-modification inside transparent materials by femtosecond laser single beam," Mod. Phys. Lett. B **19**(05), 225–238 (2005).
47. R. Taylor, C. Hnatovsky, and E. Simova, "Applications of femtosecond laser induced self-organized planar nanocracks inside fused silica," Laser Photonics Rev. **2**(1–2), 26–46 (2008).
48. D. Wortmann, J. Gottmann, N. Brandt, and H. Horn-Solle, "Micro- and nanostructures inside sapphire by fs-laser irradiation and selective etching," Opt. Express **16**(3), 1517–1522 (2008).
49. S. Richter, C. Miese, S. Döring, F. Zimmermann, M. J. Withford, A. Tünnermann, and S. Nolte, "Laser induced nanogratings beyond fused silica - periodic nanostructures in borosilicate glasses and ULE™," Opt. Mater. Express **3**(8), 1161–1166 (2013).
50. F. Zimmermann, A. Plech, S. Richter, A. Tünnermann, and S. Nolte, "Ultrashort laser pulse induced nanogratings in borosilicate glass," Appl. Phys. Lett. **104**(21), 211107 (2014).
51. T. Asai, Y. Shimotsuma, T. Kurita, A. Murata, S. Kubota, M. Sakakura, K. Miura, F. Brisset, B. Poumellec, and M. Lancry, "Systematic control of structural changes in GeO_2 glass induced by femtosecond laser direct writing," J. Am. Ceram. Soc. **98**(5), 1471–1477 (2015).
52. M. Lancry, F. Zimmerman, R. Desmarchelier, J. Tian, F. Brisset, S. Nolte, and B. Poumellec, "Nanogratings formation in multicomponent silicate glasses," Appl. Phys. B **122**(3), 66 (2016).
53. S. S. Fedotov, R. Drevinskas, S. V. Lotarev, A. S. Lipatiev, M. Beresna, A. Čerkauskaitė, V. N. Sigaev, and P. G. Kazansky, "Direct writing of birefringent elements by ultrafast laser nanostructuring in multicomponent glass," Appl. Phys. Lett. **108**(7), 071905 (2016).
54. P. Karpinski, V. Shvedov, W. Krolikowski, and C. Hnatovsky, "Laser-writing inside uniaxially birefringent crystals: fine morphology of ultrashort pulse-induced changes in lithium niobate," Opt. Express **24**(7), 7456–7476 (2016).
55. F. Zimmermann, M. Lancry, A. Plech, S. Richter, B. H. Babu, B. Poumellec, A. Tünnermann, and S. Nolte, "Femtosecond laser written nanostructures in Ge-doped glasses," Opt. Lett. **41**(6), 1161–1164 (2016).
56. E. Bricchi and P. G. Kazansky, "Extraordinary stability of anisotropic femtosecond direct-written structures embedded in silica glass," Appl. Phys. Lett. **88**(11), 111119 (2006).
57. M. Beresna, M. Gecevičius, and P. G. Kazansky, "Polarization sensitive elements fabricated by femtosecond laser nanostructuring of glass," Opt. Mater. Express **1**(4), 783–795 (2011).
58. M. Beresna, M. Gecevičius, M. Lancry, B. Poumellec, and P. G. Kazansky, "Broadband anisotropy of femtosecond laser induced nanogratings in fused silica," Appl. Phys. Lett. **103**(13), 131903 (2013).
59. M. Born and E. Wolf, *Principles of Optics* (Cambridge University, 1999).
60. A. Champion and Y. Bellouard, "Direct volume variation measurements in fused silica specimens exposed to femtosecond laser," Opt. Mater. Express **2**(6), 789–798 (2012).
61. A. Champion, M. Beresna, P. Kazansky, and Y. Bellouard, "Stress distribution around femtosecond laser affected zones: effect of nanogratings orientation," Opt. Express **21**(21), 24942–24951 (2013).
62. B. McMillen and Y. Bellouard, "On the anisotropy of stress-distribution induced in glasses and crystals by non-ablative femtosecond laser exposure," Opt. Express **23**(1), 86–100 (2015).
63. C. Hnatovsky, D. Grobnic, and S. J. Mihailov, "Nonlinear photoluminescence imaging applied to femtosecond laser manufacturing of fiber Bragg gratings," Opt. Express **25**(13), 14247–14259 (2017).
64. D. Grobnic, C. Hnatovsky, and S. J. Mihailov, "Low loss Type II regenerative Bragg gratings made with ultrafast radiation," Opt. Express **24**(25), 28704–28712 (2016).
65. S. Richter, M. Heinrich, S. Döring, A. Tünnermann, and S. Nolte, "Formation of femtosecond laser-induced nanogratings at high repetition rates," Appl. Phys., A Mater. Sci. Process. **104**(2), 503–507 (2011).
66. T. Erdogan and V. Mizrahi, "Characterization of UV-induced birefringence in photosensitive Ge-doped silica optical fibers," J. Opt. Soc. Am. B **11**(10), 2100–2105 (1994).
67. A. M. Vengsarkar, Q. Zhong, D. Inniss, W. A. Reed, P. J. Lemaire, and S. G. Kosinski, "Birefringence reduction in side-written photoinduced fiber devices by a dual-exposure method," Opt. Lett. **19**(16), 1260–1262 (1994).
68. N. Belhadj, Y. Park, S. Larochelle, K. Dossou, and J. Azaña, "UV-induced modification of stress distribution in optical fibers and its contribution to Bragg grating birefringence," Opt. Express **16**(12), 8727–8741 (2008).

1. Introduction

The preferred and by far most common method to fabricate fiber Bragg gratings (FBGs) is to use intense laser radiation in order to induce periodic or quasiperiodic changes in the refractive index of the fiber core. Interestingly, by introducing just a single phase defect – typically a π-phase shift – in the middle of an otherwise regular FBG, a very narrow transmission peak can be produced within its main stopband. Due to this special spectral feature, phase-shifted FBGs are widely used in distributed-feedback fiber lasers [1,2], optical sensors designed for pressure, strain and torsion measurements [3–6], sensitive ultrasonic detectors [7], and optical signal processing [8–10].

Traditionally, phase-shifted FBGs are fabricated by exposing the fiber to the ultraviolet (UV) radiation of excimer or frequency-doubled Ar-ion lasers [11]. The main UV laser writing techniques include the use of a special phase-shifted mask [12], precisely displacing a

Optics EXPRESS

uniform phase mask and the fiber with respect to each other during the process of FBG inscription [13], and post-processing of the FBG produced with a uniform mask [11].

Alternatively, phase-shifted FBGs can be fabricated using infrared (IR) femtosecond (fs) lasers. The primary techniques in this case are based on point-by-point/line-by-line writing [6,14,15] and displacing a uniform phase mask during the inscription [16,17]. Uniform phase masks were also used to produce phase-shifted FBGs when i) a uniform FBG was overexposed in the center [18], ii) the central part of the fs-laser beam was blocked [19] and iii) a uniform FBG was written in a length of fiber that incorporates a fusion splice [20]. Generally, the mask technique is faster, more accurate and more robust compared with the point-by-point technique. The latter, however, is much more flexible and thus allows one to more easily fabricate complex FBGs.

IR fs-laser technology has a great advantage over its UV counterpart as Bragg gratings can now be inscribed in almost any optical fiber without the need to photosensitize the fiber core [21]. Moreover, if the IR fs-pulses are focused sufficiently tightly, inscription through the protective coating ('trans-jacket inscription') becomes possible [22–29]. This allows one to avoid the removal of the protective coating and, if it is needed, its reapplication after grating inscription. These steps are undesirable from a manufacturing perspective because they are time consuming, introduce structural flaws to the fiber surface and weaken the strength and degrade long-term reliability of the resultant FBG [30,31].

In this work, we demonstrate that π-phase-shifted FBGs can be fabricated in a single step using an IR fs-laser and a special phase mask where one half of the uniform mask is shifted with respect to the other by 5/4 of the mask period. More specifically, we concentrate on the fabrication of stable Type II π-phase-shifted FBGs that can be used for highly precise measurements of temperature, strain and vibration at temperatures up to ~1000°C. This task is non-trivial because the presence of Type II modification in an FBG makes it lossy and birefringent [32]. As far as Type II π-phase-shifted FBGs are concerned, the increased optical loss associated with Type II gratings spectrally broadens the π-feature while the birefringence, depending on its magnitude, either broadens the π-feature or even splits it into two components [3,5,6]. Obviously, the ultimate accuracy and resolution of sensing measurements based on the π-feature decreases because of this broadening. Additionally, the interference pattern behind a π-phase-shifted phase mask contains a V-shaped region, which has its apex at the π-phase-shift on the surface of the mask and divides the interference fringe system into three distinct sub-regions [34,35]. The interference fringes inside the V-shaped region are shifted by + π/2 and -π/2 with respect to the fringes formed to the left and right of it. An FBG inscribed with such a pattern has an asymmetric spectrum [34,36], which makes locking to the π-feature for sensing applications more difficult.

Whereas optical loss associated with Type II modification depends on the FBG characteristics (e.g., FBG length and strength), we find that the birefringence of the Type II π-phase-shifted FBGs can be easily controlled by the fs-laser polarization. The birefringence is minimized when the linear laser polarization is aligned parallel to the fiber axis and maximized when the polarization is perpendicular to the fiber axis. We attribute this result to the presence of light-induced nanostructures in Type II FBGs [37]. We also experimentally measure and reconstruct the interference pattern behind the π-phase-shift of a 1st- and 3rd-order phase mask and in each case observe a V-shaped region which has its apex at the π-phase-shift of the mask and divides the interference pattern into three distinct sub-regions, as predicted [35]. The presence of the V-shaped region causes a pronounced asymmetry in the spectra of FBGs written with the 1st-order mask. We show that this asymmetry can be corrected by covering the π-phase-shift region of the mask with a rectangular beam stop and choosing the correct mask-to-fiber distance based on the transverse and longitudinal walk-off of the diffracted fs-beams [28,38,39].

Optics EXPRESS

2. Background

2.1 Light intensity distribution after a π-phase-shifted mask

Interference patterns produced with fs-pulses and a uniform phase mask (i.e., phase diffraction grating) are well-studied both theoretically and experimentally [28,38,39]. Consider an ideal situation when the mask (**M** in Fig. 1(a)) splits the incident light only into + 1 and −1 diffraction order, as schematically presented in Fig. 1(a). A pure two-beam interference pattern is then formed in region I, whereas the intensity distribution is fringeless in regions II and III. It can also be seen that the intensity distribution at the fiber (**F**) will be strongly affected by both the effective width *2w* of the fs-beam at **M** (e.g., the diameter at the

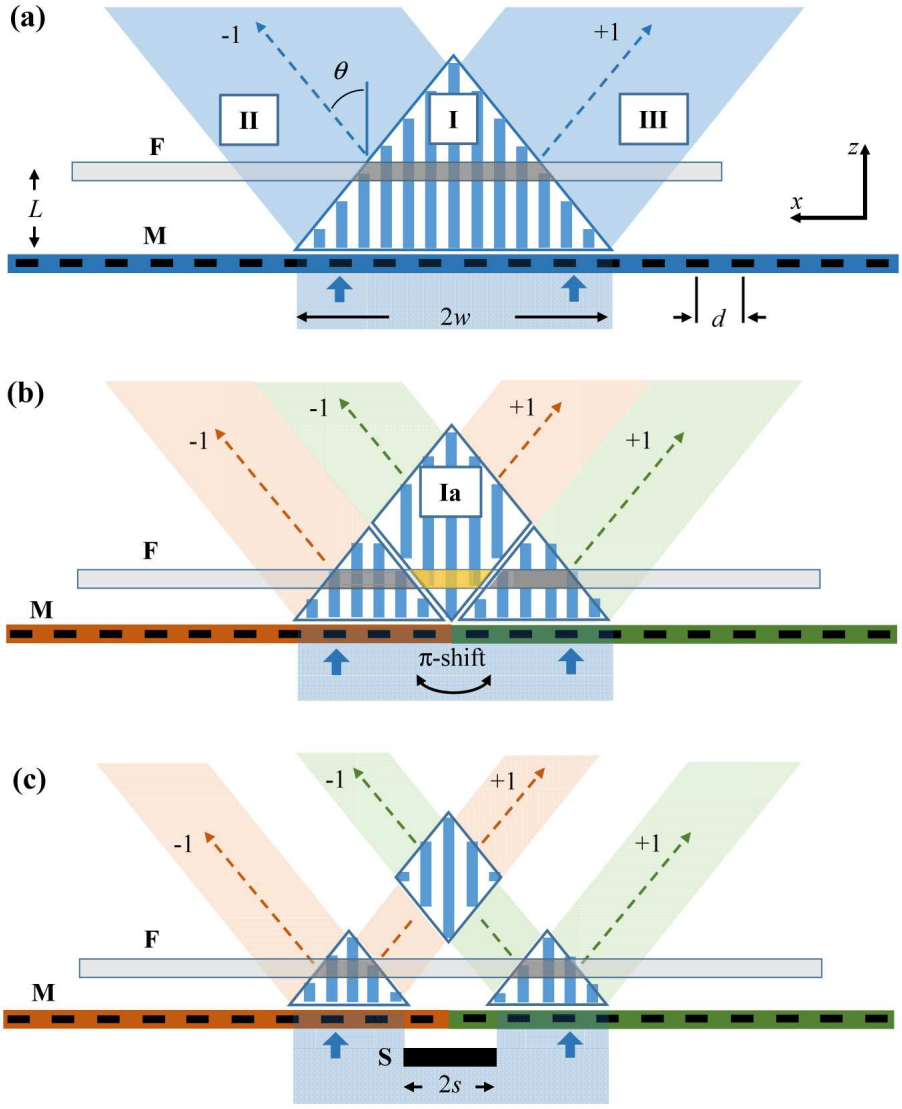

Fig. 1. Regions where ultrashort pulses produce interference patterns after a phase mask (**M**) that diffracts light only into ± 1 orders. (a) A uniform phase mask. (b) A π-phase-shifted phase mask. (c) A π-phase-shifted phase mask when the central portion of the laser beam is obstructed by a rectangular stop (**S**) of width 2*s*. An optical fiber (**F**) is at a distance *L* from (**M**). The diffraction angle is θ ; the effective beam width is 2*w*.

Optics EXPRESS

$1/e^2$ intensity level for a fs-beam with a Gaussian intensity profile) and the mask-to-fiber distance L.

Now we consider a uniform phase mask containing a phase-shift. In the simplest case, the introduction of a single phase shift into a uniform phase mask of pitch d can be thought of as cutting it into two sections and then inserting (or removing) material of width δ between the two sections. Hereinafter, a 'π-phase-shifted mask' is defined as a uniform phase mask one half of which is shifted with respect to the other by 5/4 of the mask period d, i.e., $\delta = d/4$. The 'π-shift' terminology originates from the fact that a phase shift with $\delta = d/4$ in the middle of a uniform phase mask causes a phase-shift of $2\pi\delta/(d/2) = \pi$ in the resultant FBG, whose period is $d/2$ by definition.

If a phase shift is introduced into **M**, the interference pattern produced after it becomes more complicated compared with the one presented in Fig. 1(a). In the case of a π-phase shift ('π-shift' in Fig. 1(b)), the + 1 diffraction order of the **M**'s left half (shown in orange in Fig. 1(b)) and the −1 diffraction order of the **M**'s right half (shown in green in Fig. 1(b)) can now generate an additional interference fringe system within region I, which divides it into three sub-regions. The interference fringes within sub-region Ia are shifted with respect to the fringes in the left and right triangular sub-regions by π/2, i.e., by a quarter of the fringe period [35]. The boundaries of the sub-regions are defined by **M** and the diffraction angle θ.

When the fiber intercepts all of the three sub-regions, the light-imprinted structure inside it will consist of three sections with a π/2-shift between the adjacent sections. The length of the central section (in yellow) and each of the two side sections (in grey), provided that the fiber is aligned along the x-axis, can be approximated by $2L\tan(\theta)$ and $w\text{-}2L\tan(\theta)$, respectively.

The presence of the central section causes an asymmetry in the FBG spectra, as demonstrated in Fig. 2 using simulation software (OptiGrating, Optiwave Inc., Nepean, ON, Canada). A detailed analysis of why the π-features in the spectra are shifted to shorter wavelengths is provided in [36].

We consider a phase mask with a pitch d = 1.07 μm (i.e., a phase mask to inscribe FBGs with the 1st-order resonance at ~1.55 μm in SMF-28 fiber). For fs-laser radiation centered at λ = 800 nm the diffraction angle $\theta = \arcsin(\lambda/d)$ is large (i.e., θ ~48.5°) and the contribution of the central section can be quite significant. For example, for L = 0.5 mm and a fs-beam with $2w$ = 7 mm, the length of the central section at the fiber core is ~1.1 mm, whereas the length of the side sections is ~2.4 mm. Also, we consider a fs-beam with a quasi-flat-top intensity profile (see the 'Experimental' section) and, as a result, assume the light-induced refractive index modulation Δn in the central and side sections to be the same. For the same reason, the effective refractive index of the fiber core n_{eff} in the central and side sections is also assumed to be the same. For $\Delta n = 5\cdot10^{-4}$ and n_{eff} = 1.447, a strong asymmetry in the spectrum is produced, as shown in the blue plot in Fig. 2(a). For L = 0.25 mm, the length of the central section at the fiber core decreases to ~0.55 mm and the length of the side sections increases to ~2.9 mm. The asymmetry in the spectrum under these writing conditions is weaker than in the previous case but is still quite noticeable (red plot in Fig. 2(a)). Obviously, to reduce the contribution of the central section it has to be made short relative to the side sections, which can be achieved, for instance, by expanding the beam along the fiber to increase $2w$, minimizing L, and using a higher order mask (e.g., a 3rd-order mask instead of a 1st-order mask) to decrease θ.

Optics EXPRESS

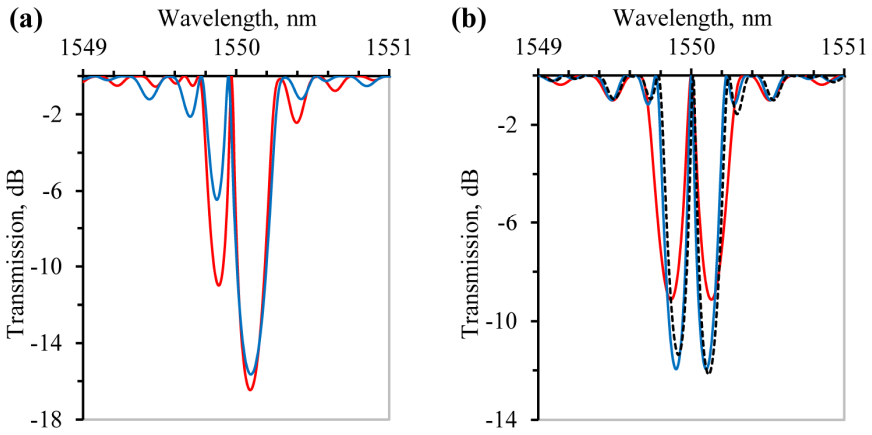

Fig. 2. Spectral characteristics of FBGs produced with a π-phase-shifted mask under different laser writing conditions. In the simulations (Optiwave software), the mask pitch d is 1.07 μm, the effective refractive index of the fiber core n_{eff} is = 1.447, the light-induced refractive index modulation in the core Δn is $5 \cdot 10^{-4}$. (a) FBG spectra corresponding to the case shown in Fig. 1(b). The blue plot represents L = 0.5 mm, with the length of the central section and side sections at the fiber core being 1.1 mm and 2.4 mm, respectively. The red plot represents L = 0.25 mm, with the length of the central section and side sections at the fiber core being 0.55 mm and 2.9 mm, respectively. (b) Spectra corresponding to the case shown in Fig. 1(c) when L = 0.25 mm and $2s$ = 1 mm. The blue plot represents a π-shifted Fabry-Pérot interferometer composed of two detached 2.4 mm-long uniform Bragg gratings with a 1.6 mm separation between them. The black plot (dashes) shows how the spectrum of the above interferometer is changed when n_{eff} in the two detached π-shifted FBGs is higher than in the central unexposed section by $5 \cdot 10^{-5}$. The red plot represents a standard 4.8 mm-long π-shifted FBG.

Alternatively, the central part of the fs-beam can be obscured by a rectangular stop (**S**) of width $2s$, as shown in Fig. 1(c). In this case, the additional interference fringe system described earlier can be moved away from the mask and a π-shifted Fabry-Pérot interferometer composed of two detached Bragg gratings inscribed into the fiber by choosing a proper mask-to-fiber distance L. The two Bragg gratings will always be π-shifted with respect to each other because they are produced by interference patterns that are π-shifted by definition (the fringes are 'affixed' to the mask). It can be shown using simulations (Fig. 2(b)) that such a fiber interferometer will spectrally resemble a standard π-shifted FBG if the separation between the two constituting FBGs, which is given by $2(s + L\tan(\theta))$, remains smaller than their length, which is respectively given by $w\text{-}s\text{-}2L\tan(\theta)$. The linear dimensions of the π-shifted Fabry-Pérot interferometer whose spectrum is shown in Fig. 2(b) are calculated based on the above expressions and a 7 mm width (i.e., $2w$) of the quasi-flat-top fs-beam.

Strictly speaking, for the above consideration to be valid, one has to assume that n_{eff} is not affected by the inscription process. In reality, n_{eff} in the laser-irradiated regions and the unexposed portions of the fiber is different, which also causes an asymmetry in the FBG spectrum. If n_{eff} in the irradiated regions is higher/lower than that in the unexposed fiber core, the π-feature moves towards shorter/longer wavelengths within the FBG spectrum. The dashed black trace in Fig. 2(b) demonstrates the situation when n_{eff} in the two detached π-shifted FBGs of the Fabry-Pérot interferometer is higher than in its central unexposed section by $5 \cdot 10^{-5}$, i.e., $0.1 \cdot \Delta n$. Such light-induced changes (i.e., $\Delta n_{eff} = (0.1\text{-}0.3) \cdot \Delta n$) are typical of FBGs produced using IR fs-lasers [40]. One can see that the spectral asymmetry in the dashed black trace in Fig. 2(b) is significantly smaller than in the red trace in Fig. 2(a).

We note that, in principle, the above 'beam-stop technique' may also be used with standard uniform masks to produce π-shifted Fabry-Pérot interferometers if the unexposed region at the fiber core happens to introduce the correct phase shift between the two detached

Optics EXPRESS

Bragg gratings [19]. Taking into account that in this case the phase shift critically depends on the length of the unexposed region, the latter has to be somehow adjusted to a fraction of a micrometer to produce a symmetric spectrum.

2.2 Birefringence of Type II FBGs

FBGs inscribed using IR fs-laser radiation are typically classified into two main categories, Type I and Type II gratings, which have differing degrees of resistance to high-temperature (i.e., ~1000°C) annealing [40]. It is traditionally thought that the light-induced texture inside Type I and Type II FBGs is respectively smooth and disrupted [41–43]. Recently, periodic planar nanostructures [44,45] were found in Type II Bragg gratings produced in SMF-28 fiber by side-illuminating it with multiple linearly polarized IR fs-laser pulses through a phase mask [37]. Similar nanostructures were also observed in many different transparent bulk materials [46–55].

The planar nanostructures, which are often referred to as nanogratings, are aligned perpendicular to the linear laser polarization and exhibit strong form birefringence [33,56–58]. Form birefringence is observed in a periodically layered medium when the spacing between the layers is small compared with the wavelength of light [59]. In this case the medium behaves as an optically uniaxial crystal whose optical axis is oriented perpendicular to the layers. The refractive index difference between the ordinary and extraordinary rays in fs-laser-induced nanostructures can be as high as $5 \cdot 10^{-3}$ [56].

Additionally, it was shown that nanogratings are responsible for a deformation in the host material on the order of ~0.03%, and that this deformation (and associated stress) is largest in the direction perpendicular to the nanograting planes, i.e., parallel to the linear beam polarization [60]. Because of photoelasticity, anisotropic stress caused by the presence of nanograting structures induces birefringence inside them and the surrounding material, with the optical axis of such an optically anisotropic medium being parallel to the dominant stress component [61,62].

As a consequence of the above two effects, i.e., form birefringence and stress birefringence, the spectral characteristics of a (π-shifted) Bragg grating whose planes contain nanostructures will depend on how the nanostructures are oriented with respect to the fiber. The FBG spectrum is expected to be least sensitive to the polarization state of the probe light propagating through it when the planar nanostructures are aligned perpendicular to the fiber. Indeed, in this case both the uniaxial form-birefringent crystal associated with the subwavelength periodic structure of nanogratings and the uniaxial stress-birefringent crystal induced by the deformation in the material due to nanogratings have their optical axes aligned parallel to the fiber core. For such a geometry, the effective refractive index of the core for different states of polarization of the probe light is the same. Thus, in order to avoid or minimize the polarization dependence of the FBG spectrum, the polarization of the fs-laser pulses should be aligned parallel to the fiber axis. Conversely, in order to maximize both the form birefringence and stress birefringence of (π-shifted) Type II FBGs, which is desirable for some applications [6], the fs-laser polarization should be aligned perpendicular to the fiber. Under such writing conditions, optical axes of the form-birefringent crystal and the stress-birefringent crystal are aligned perpendicular to the fiber core and the FBG can be thought of as a (multiple-order) wave plate in terms of its birefringent properties. If other orientations of the linear polarization are used for the inscription, the resultant planar nanostructures are produced at an angle with respect to the fiber core and the birefringence attains an intermediate value.

3. Experiment

A schematic of the inscription set up used to write the phase-shifted FBGs is presented in Fig. 3. An 80 fs Ti-sapphire regenerative amplifier operating at a central wavelength of λ = 800 nm was used in the experiments. The linearly polarized output Gaussian beam ~7 mm in

Optics EXPRESS

diameter at the $1/e^2$ intensity level was expanded ~3 times along the x-axis and focused through a π-shifted phase mask (**M**; the pitch either 1.07 μm or 3.21 μm; the masks were fabricated using standard e-beam photolithography) using a plano-convex acylindrical lens (**CL**; focal distance 12 mm; the curved surface of **CL** is designed to reduce spherical aberration in one dimension), with the resultant line-shaped laser focus being aligned parallel to the fiber axis (Fig. 3(a)). A rectangular aperture (**A**) (i.e., a slit) aligned along the y-axis was placed between **CL** and **M**, as depicted in Fig. 3(a).

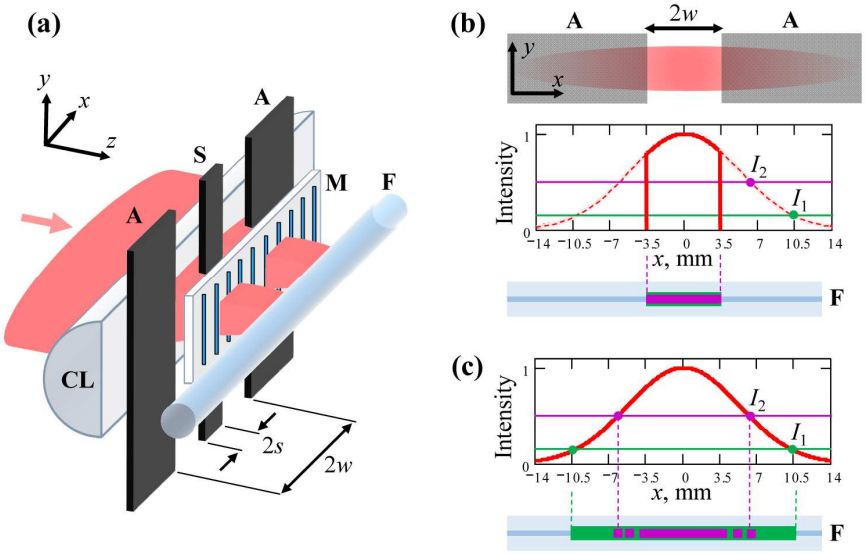

Fig. 3. Inscription of π-phase-shifted FBGs using the phase mask technique. (a) A schematic of the setup. **CL** is an acylindrical lens; (**A**) is an aperture to select the central part of the fs-beam and make it quasi-flat-top along the x-axis; (**S**) is a rectangular stop to obstruct the central portion of the beam in order to not allow any light to impinge the π-phase shift on (**M**) (see text). (b) A fs-beam with a quasi-flat-top intensity profile of width $2w$ = 7 mm along the x-axis induces a 7 mm Type II modification (purple) in the fiber core. (c) When (A) is removed from the fs-beam path the resultant FBG consists of both Type I (green) and Type II (purple) modification.

Consider a situation when **A** is centered relative to the fs-beam along the x-axis (Fig. 3(b)). We also assume that the width of **A**, which is denoted by $2w$, is significantly smaller than the beam width along the x-axis at the $1/e^2$ intensity level. If the distance from **A** to **M** along the z-axis is not too large compared with $2w$, diffraction effects at **A** can be neglected [28] and the light intensity distribution at **M** (and **F**) along the x-axis becomes quasi-flat-top, as schematically presented in red in Fig. 3(b). By keeping the peak light intensity in the line shaped fs-laser focus well above the intensity threshold to induce Type II modification in the fiber core [40], which is denoted by I_2, a FBG consisting of well-delineated Type II modification (shown in purple) and Type I modification (shown in green) can be produced. At the operating temperature, i.e., at 700-1000°C, Type I modification in the material is dramatically reduced or completely erased due to annealing [42,43] and a uniform Type II FBG is thus created. Without **A**, the intensity distribution at **F** along the x-axis will be Gaussian (Fig. 3(c)). As a result, the FBG in this case will consist of Type I modification at the ends, where the intensity is higher than the threshold intensity I_1 to induce Type I modification, but lower than I_2, and Type I and Type II modification in the center, where the peak intensity is higher than I_2. Type I and Type II modification can also intermingle in the regions where the intensity is close to I_2 [37]. After exposing this FBG to high temperatures, the Type I modification will be erased and the FBG spectrum will become determined by a rather complex distribution of the remaining Type II modification, which can be intermittent

Optics EXPRESS

and asymmetric with respect to the π-shift. To avoid this issue, **A** was always used during the inscription. Using IR induced photoluminescence in the fiber [63], the line focus was centralized in the fiber core along the y-axis. During grating inscription the beam was not scanned across the fiber in the y-direction.

3.1. Inscription of π-shifted Type II FBGs in SMF-28-type fiber using a first-order mask

The averaged *xz*-intensity distributions of the femtosecond pulses after a π-shifted phase mask with a 1.07 μm pitch are presented in Fig. 4(a) and Fig. 4(b). Figure 4(a) shows the distribution in the vicinity of the π-shift (the π-shift is at $x = 0$, $z = 0$; region Ia in Fig. 1(c)), whereas Fig. 4(b) shows the distribution 500 μm away from it along the *x*-axis. For the reasons discussed below, the *z*-range of the images in Fig. 4(a) and Fig. 4(b) is also different. To produce the images, the respective *xy*-intensity distributions with a 1 μm separation along the *z*-axis were projected onto a CMOS matrix by means of a high numerical aperture (i.e., NA = 0.9) objective lens, recorded and combined into 3D stacks [63]. The values of points with fixed (x_i, z_i) coordinates were then averaged along the *y*-axis and the respective mean values projected onto the *xz*-plane in order to minimize the ~10-times difference in brightness between the intrafocal and out-of-focus regions along the *z*-axis. As a matter of fact, the focal plane of **CL** is at z ~50 μm in Fig. 4(a) and at z ~250 μm in Fig. 4(b).

The most salient feature of the intensity distribution in Fig. 4(a) is the pronounced V-shaped region whose apex coincides with the π-shift [34]. The angle at the apex is estimated at 90-95°. This value is close to twice the diffraction angle $\theta = \arcsin(\lambda/d)$ corresponding to λ = 800 nm and d = 1.07 μm, as predicted [35]. The clear Talbot interference pattern observed in Fig. 4(a), especially at $z < 50$ μm, is caused by the presence of the 0th diffraction order, which we neglected in the 'Background' section. In reality, the 0th order always contains a certain portion of the incident laser power, albeit it can be as low as 1% for state-of-the-art holographic masks. As a consequence, the contrast of the Talbot pattern generated by a 1st-order mask depends on the ratio of laser powers diffracted into the 1st and 0th order and the longitudinal walk-off of the orders [28,38,39]. This power ratio can be varied within a broad range by selecting the mask design, but for a given design it will also be affected by the pulse polarization. For consistency, all the images in Fig. 4 and Fig 6 were obtained using the pulse polarization aligned along the *x*-axis.

Fig. 4.(b) represents the case when the separation between the 0th and 1st diffraction order along the *z*-axis (i.e., longitudinal walk-off) is sufficiently large and, as a result, pulses diffracted into the + 1 and −1 orders produce a classic two-beam interference pattern.

Following the discussion in the 'Background' section, in Fig. 5(a) we demonstrate that the presence of a wide-angle V-shaped feature in the intensity distribution after a 1.07 μm pitch mask results in a quite large asymmetry in the FBG spectrum when the mask-to-fiber distance L is ~450 μm (see Fig. 1), as expected. Importantly, the asymmetry almost disappears when a ~1 mm wide rectangular stop **S** (Fig. 1 and Fig. 3) is inserted to cover the π-shift and thus eliminate the additional interference fringe pattern at the fiber core, as shown in Fig. 5(b).

Optics EXPRESS

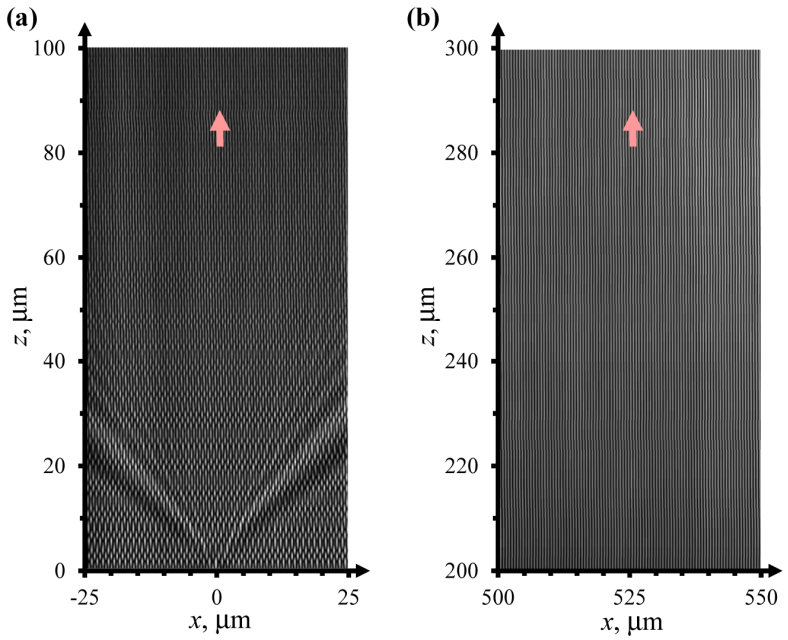

Fig. 4. Interference patterns produced by 80 fs pulses after a π-phase-shifted mask with a 1.07 μm pitch. The mask is at $z = 0$. While recording the images, the laser power was kept at a ~1 mW level and the pulse repletion rate was 1 kHz. (a) The pattern in the vicinity of the π-shift (x = 0, z = 0). (b) The pattern 500 μm away from the π-shift along the x-axis. The different z-ranges in (a) and (b) are used to demonstrate that a Talbot-type interference pattern is formed near the mask, while a two-beam interference pattern is formed at $z > 200$ μm.

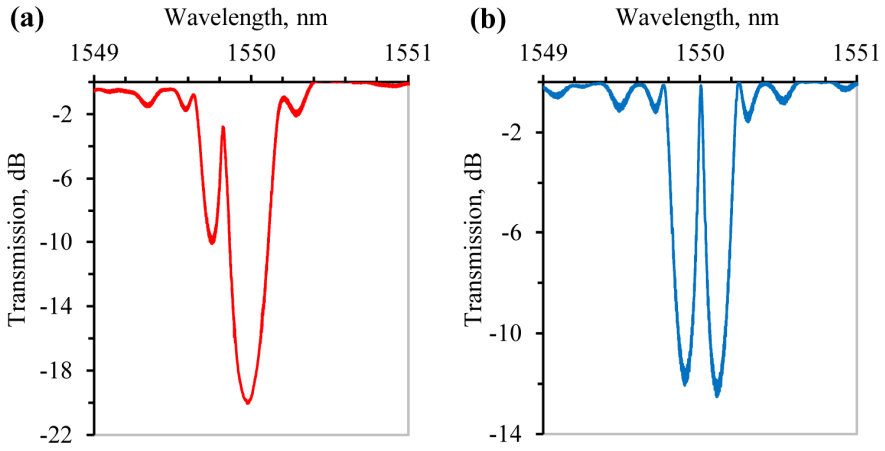

Fig. 5. Spectral asymmetry of π-shifted FBGs produced by a π-phase-shifted mask and a method to correct this asymmetry. The mask pitch d is 1.07 μm. (a) The spectrum of an FBG written at L ~450 μm when the fiber core was exposed to a complex interference pattern consisting of three regions (see Fig. 1(b)). (b) The spectrum of an FBG written at L ~450 μm when the π-shift is blocked by a stop (**S**) with $2s$ ~1 mm (see Fig. 1(c)). The FBG in (b) becomes a π-shifted Fabry-Pérot interferometer composed of two detached uniform Bragg gratings. The laser parameters in (a) and (b) are the same. The spectra were recorded using a tunable laser source with a 1 pm resolution.

To produce these Type II Bragg gratings we irradiated a polyimide-coated SMF-28-type fiber with ~10 80 fs pulses at a 1 Hz pulse repetition rate. The alignment of the line-shaped laser focus with respect to the fiber core was performed using the nonlinear microscopy

Optics EXPRESS

technique described in Refs [28,63]. The pulse energy used for the inscription was approximately 3.5 times the pulse energy threshold required to induce Type II modification in this fiber under otherwise the same writing conditions. The pulse polarization was aligned along the fiber, i.e., along the *x*-axis.

3.2. Inscription of π-shifted Type II FBGs in SMF-28 fiber using a third-order mask

The results from the previous section demonstrate that by blocking the π-shift one can fabricate quite symmetric Type II FBGs using a 1st-order mask, even when the inscription is performed at some distance from the mask, i.e., at L ~450 μm. However, our previous results demonstrated that the long-term stability of Type II FBGs at high temperatures (i.e., ~1000°C) was improved when a 3rd-order mask was used for the inscription [64]. Taking into account the fact that this paper focuses on stable π-shifted Type II FBGs for extreme environments, the remainder is dedicated to studying the properties of gratings produced with a 3.21 mm pitch mask. Additionally, the use of a high-order mask has another advantage. As can be seen in Fig. 6(a), the apex angle of the V-shaped feature is ~3 times smaller than in the case of the 1.07 μm pitch mask (Fig. 4(a)) and at convenient mask-to-fiber distances in the range of 200-500 μm there is no need to use a beam stop **S** any longer. To be consistent with the previous section, in Fig. 6(b) we also show the averaged *xz*-intensity distributions 500 μm away from the π-shift along the *x*-axis. In this case, however, the longitudinal walk-off of the 0th, 1st, 2nd and 3rd diffraction orders is small and instead of a two-beam interference pattern shown in Fig. 4(b) a Talbot-type interference pattern is formed.

As in the previous section, 80 fs pulses at a 1 Hz repetition rate were used during the FBG inscription process. In this case, however, the FBGs were produced inside stripped SMF-28 fiber (i.e., the acrylic protective coating was removed). The fiber was placed at L ~300 μm from the mask. The pulse energy was the same as the one that we used to produce π-shifted Type II FBGs with the 1.07 μm pitch mask. For the 3.21 μm pitch mask, however, the 1.55 μm wavelength corresponds to the 3rd-order Bragg resonance and in order to keep the FBG strength at the level of 10-15 dB (in transmission) the number of pulses deposited into the fiber had to be increased to ~20-25, to enhance the refractive index modulation Δn in the fiber core. Additionally, two orientations of the linear pulse polarization – along the fiber (x-polarization) and perpendicular to the fiber (y-polarization) – were used for the inscription to investigate whether the pulse polarization had any effect on the spectral properties of the π-shifted Type II FBGs. We note that for the 3.21 μm pitch mask the diffraction efficiency into different orders varied with polarization only slightly (relative change was < 3% for the 1st order). The results of these studies are presented in Fig. 7.

Figure 7(a) clearly demonstrates that the y-polarization produces highly birefringent FBGs. In this work, the polarization-dependent difference in the central wavelength (PD-λ) of the π-feature is almost 70 pm. The three plots in Fig. 7(a) correspond to different states of the probe light polarization (i.e., $\mathbf{p_s}$, $\mathbf{p_f}$ and $\mathbf{p_{45}}$), which were prepared by means of an in-line polarization controller. The blue and red traces represent the situations when the probe light is linearly polarized and the polarization is aligned along the slow axis ($\mathbf{p_s}$; 'large' n_{eff}) and the fast axis ($\mathbf{p_f}$; 'small' n_{eff}) of the FBG, respectively. The black trace represents the case when the linear polarization is at 45° with respect to the axes (i.e., $\mathbf{p_{45}}$).

Optics EXPRESS

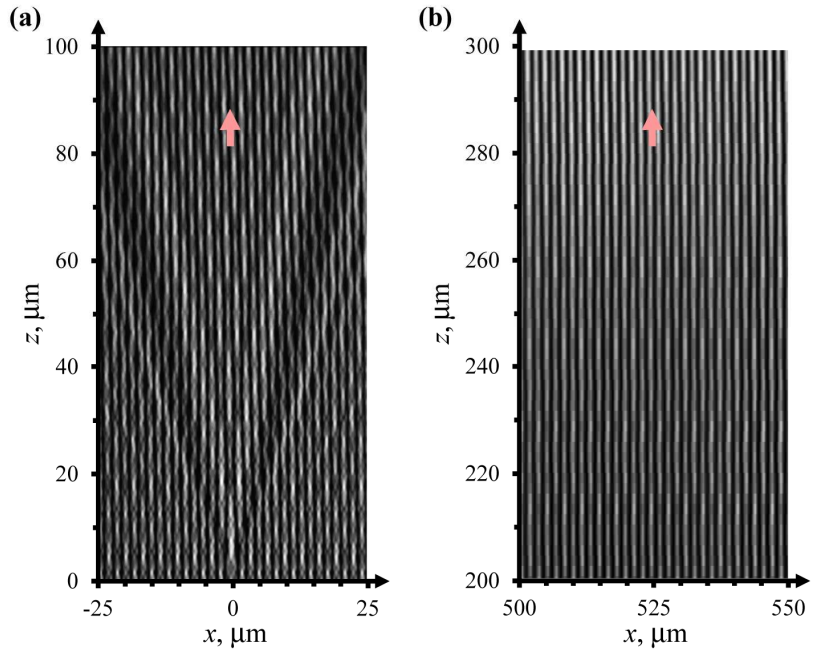

Fig. 6. Interference patterns produced by 80 fs pulses after a π-phase-shifted mask with a 3.21 μm pitch. The mask is at $z = 0$. While recording the images, the laser power was kept at ~1 mW level and the pulse repletion rate was 1 kHz. (a) The pattern in the vicinity of the π-shift (x = 0, z = 0). (b) The pattern 500 μm away from the π-shift along the *x*-axis. The longitudinal walk-off of the 0th, 1st, 2nd and 3rd diffraction orders for the *z*-range in (b) is insufficient to ensure a two-beam interference pattern (see Fig. 4(b) for comparison).

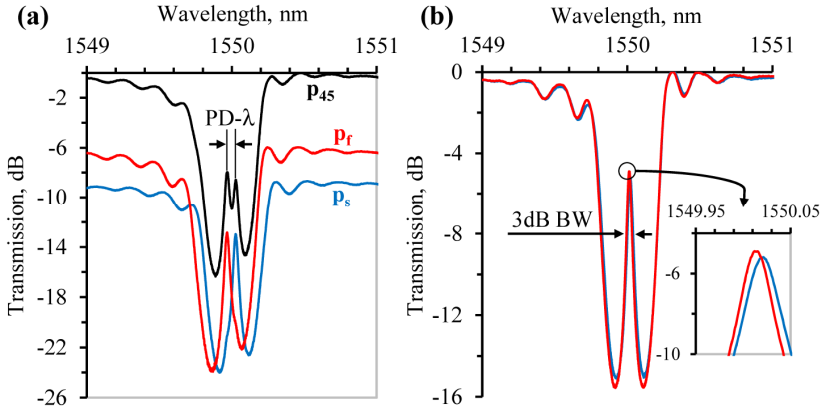

Fig. 7. Birefringence of fs-laser-written π-shifted Type II FBGs and its dependence on the fs-laser polarization. (a) The fs-laser polarization is aligned perpendicular to the fiber (y-polarization). The polarization-dependent wavelength shift of the π-feature (i.e., PD-λ) is ~70 pm. (b) The fs-laser polarization is aligned along the fiber (x-polarization). In the insert to (b): PD-λ is ~8 pm; 3 dB band width (i.e., 3 dB BW) of the π-feature is ~35 pm. The same writing conditions except for the fs-laser polarization were used for the FBGs presented in (a) and (b). The spectra were recorded using a tunable laser source with a 1 pm resolution.

On the other hand, the FBG written with the x-polarization (Fig. 7(b)) shows almost an order of magnitude smaller PD-λ (i.e., 7-8 pm), with all other laser writing conditions being the same in both cases. Importantly, the PD-λ of 10-15 dB π-shifted Type I FBGs is found to be much smaller, at the level of 1-2 pm for x-polarization and 3-5 pm for y-polarization. These results suggest that the observed polarization sensitivity of the Type II FBG spectra

Optics EXPRESS

(i.e., PD-λ) is caused by the presence of light-induced planar nanostructures (or nanogratings), which inside dielectrics are aligned perpendicular to the laser polarization [44,45,56,58]. It has also been shown that nanograting formation can occur with as little as a few tens of overlapping pulses [65], which represents our laser writing conditions. In the case of UV laser induced birefringence during FBG fabrication [66], the PD-λ is instead associated with a gradient in the UV-induced index change profile that traverses the core [67] and asymmetric glass densification in the photosensitive regions of the exposed fiber [68] in the absence nanogratings. Similarly, Type I FBGs written with a femtosecond laser and a phase mask were also observed to have high birefringence when the inscription laser polarization was normal to the fiber axis [32]. The relative contributions of fs-laser induced index gradients versus nanograting formation are unclear. A detailed study of the impact of the inscription IR-beam polarization on the form birefringence and PD-λ of thermally stable fs-FBGs will be presented elsewhere.

To test how π-shifted Type II FBGs written with the 3.21 μm pitch mask respond to high-temperature annealing, we fabricated tens of devices having different strength (3-30 dB in transmission), which for a fixed pulse energy increases with the number of pulses deposited into the fiber core. The devices were then temperature-cycled 20 times inside a tube furnace from 20°C to 1000°C in ambient air. During this testing, the FBGs stayed in the furnace at 1000°C for more than 200 hours. We observed that the π-features of all the FBGs tested shifted towards longer wavelength by 150-250 pm. However, this noticeable shift mainly occurred only in the first 30-50 cumulative hours of annealing at 1000°C and almost no shift could be detected during the later stages of the experiment. As an example, the high-temperature performance of an 8 dB FBG is presented in Fig. 8.

Figure 8(a) shows the spectrum (in blue) of this FBG at room temperature (i.e., T = 20°C) right after the inscription together with its spectrum (in red) at T = 1000°C after ~200 cumulative hours of annealing at this temperature. It can be seen that the FBG strength has decreased from ~8 dB to ~7 dB and the FBG spectrum has slightly changed its shape. We also note that these transformations took place during the first 25-30 cumulative hours of annealing at 1000°C after which the FBG remained unchanged. The wavelength shift of the π-feature as a function of annealing time at 1000°C is presented in Fig. 8(b). Based on these data, the FBG can be considered 'almost' stable and 'absolutely' stable after respectively ~35 and ~100 hours at 1000°C. Such a behavior is also typical of the other FBGs we used in the experiment.

Optics EXPRESS

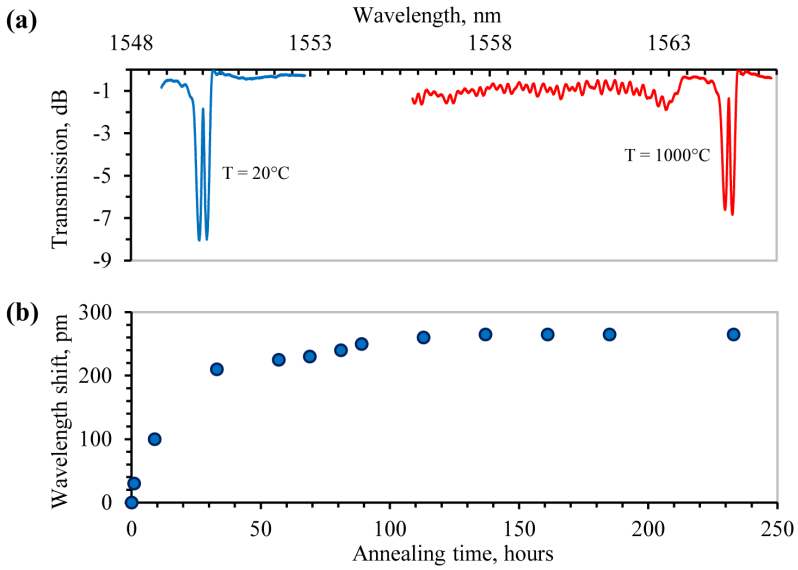

Fig. 8. High-temperature performance of fs-laser-written π-shifted Type II FBGs. (a) The blue trace shows the initial FBG spectrum at 20°C, whereas the red trace shows the spectrum at 1000°C after ~200 cumulative hours of annealing at this temperature. (b) The wavelength shift of the π-feature as a function of annealing time at 1000°C.

4. Conclusions

In this paper, we have demonstrated that π-shifted Type II FBGs can be inscribed in a single step inside a standard telecom fiber (SMF-28) using an e-beam written phase mask incorporating a π-phase shift in its center and an infrared femtosecond laser.

Despite the seeming similarity between the FBG inscription using a uniform phase mask and a phase-shifted mask, diffraction at the phase shift in the latter case leads to the formation of an interference pattern with three distinct phase-shifted regions, which we experimentally observe after a 1st- and 3rd-order π-phase-shifted mask. If such a complex pattern is imprinted into the fiber core, a Bragg grating with an asymmetric spectrum is produced. This effect is especially pronounced when inscription is performed with a 1st-order mask. However, this inherent asymmetry can be removed by covering the π-shift in the mask. By doing so, a π-shifted Fabry-Pérot interferometer composed of two equal uniform Bragg gratings can be inscribed into the fiber if a proper mask-to-fiber distance is chosen. We demonstrate these cases both numerically and experimentally. By using a 3rd-order mask there is no need to cover the π-shift for certain writing conditions.

Further, we have demonstrated that the birefringence of π-shifted Type II FBGs is strongly affected by the femtosecond laser polarization. When gratings are produced with the fs-laser (linear) polarization aligned perpendicular to the fiber, the central wavelength of the π-feature can shift by as much as 70 pm (i.e., PD-λ ~70 pm) depending on the probe light polarization. On the other hand, when the fs-laser polarization is aligned along the fiber, the birefringence of the resultant FBG and, as a consequence, the wavelength shift of the π-feature can be reduced by an order of magnitude (i.e., PD-λ ~8 pm). We attribute the birefringence of Type II FBGs to the presence of light-induced nanostructures inside the grating planes.

The π-shifted Type II FBGs fabricated with a 3rd-order phase mask using the 'optimum' fs-laser polarization have shown PD-λ in the range of 3-10 pm and a remarkable thermal stability at 1000°C at prolonged annealing intervals. Such gratings can provide a unique solution to perform high-resolution measurements of temperature, load and vibration in extreme temperature environments.